Waterless TiO$_2$ atomic layer deposition using titanium tetrachloride and titanium tetraisopropoxide

Virginia R. Anderson, Andrew S. Cavanagh, and Aziz I. Abdulagatov
Department of Chemistry and Biochemistry, University of Colorado, Boulder, Colorado 80309-0215

Zachary M. Gibbs
Department of Chemical and Biological Engineering, University of Colorado, Boulder, Colorado 80309-0424

Steven M. George[a)]
Department of Chemistry and Biochemistry, University of Colorado, Boulder, Colorado 80309-0215
and Department of Mechanical Engineering, University of Colorado, Boulder, Colorado 80309-0427.

The surface chemistry for TiO$_2$ atomic layer deposition (ALD) typically utilizes water or other oxidants that can oxidize underlying substrates such as magnetic disks or semiconductors. To avoid this oxidation, waterless or oxidant-free surface chemistry can be used that involves titanium halides and titanium alkoxides. In this study, waterless TiO$_2$ ALD was accomplished using titanium tetrachloride (TiCl$_4$) and titanium tetraisopropoxide (TTIP). *In situ* transmission Fourier transform infrared (FTIR) studies were employed to study the surface species and the reactions during waterless TiO$_2$ ALD. At low temperatures between 125 and 225 °C, the FTIR absorbance spectra revealed that the isopropoxide species remained on the surface after TTIP exposures. The TiCl$_4$ exposures then removed the isopropoxide species and deposited additional titanium species. At high temperatures between 250 and 300 °C, the isopropoxide species were converted to hydroxyl species by β-hydride elimination. The observation of propene gaseous reaction product by quadrupole mass spectrometry (QMS) confirmed the β-hydride elimination reaction pathway. The TiCl$_4$ exposures then easily reacted with the hydroxyl species. QMS studies also observed the 2-chloropropane and HCl gaseous reaction products and monitored the self-limiting nature of the TTIP reaction. Additional studies examined the waterless TiO$_2$ ALD growth at low and high temperature. Quartz crystal microbalance measurements observed growth rates of ~3 ng/cm^2 at a low temperature of 150 °C. Much higher growth rates of ~15 ng/cm^2 were measured at a higher temperature of 250 °C under similar reaction conditions. X-ray reflectivity analysis measured a growth rate of 0.55 ± 0.05 Å/cycle at 250 °C. X-ray photoelectron depth-profile studies showed that the TiO$_2$ films contained low Cl concentrations <1 at. %. This waterless TiO$_2$ ALD process using TiCl$_4$ and TTIP should be valuable to prevent substrate oxidation during TiO$_2$ ALD on oxygen-sensitive substrates. © *2014 American Vacuum Society.*
[http://dx.doi.org/10.1116/1.4839015]

I. INTRODUCTION

TiO$_2$ atomic layer deposition (ALD) has been studied very extensively. TiO$_2$ ALD can be performed using a variety of titanium and oxygen precursors. The first reported TiO$_2$ ALD chemistry utilized TiCl$_4$ and H$_2$O.[1] Other titanium precursors can be used together with H$_2$O such as titanium-tetraisopropoxide (TTIP)[2,3] and tetrakis-dimethyl-amido titanium (TDMAT).[3] Other oxidants have also been employed in addition to H$_2$O. TiO$_2$ ALD has been achieved using TTIP and hydrogen peroxide.[4] Ozone has also been used together with TTIP,[5,6] TDMAT,[7] and CpTi(OMe)$_3$.[8] Plasma-enhanced TiO$_2$ ALD has also been accomplished using an O$_2$ plasma together with a variety of titanium precursors.[9] Other TiO$_2$ ALD processes have avoided forming hydroxyl groups by employing TiI$_4$ and O$_2$.[10]

The oxygen-containing precursors used during TiO$_2$ ALD can also oxidize the starting substrate. This oxidation can degrade the performance of the device fabricated using the TiO$_2$ ALD film. For example, oxygen precursors can oxidize

and corrode cobalt in magnetic media.[11,12] Overcoats that are continuous, pinhole-free, and highly resistive are required to protect cobalt from corrosion by O$_2$ and H$_2$O.[11,12] Oxygen precursors can also oxidize semiconductor substrates and form a native oxide.[13,14] Especially for high k dielectric film stacks, this native oxide can be detrimental to the resulting film dielectric constant.[15]

One approach to avoid using H$_2$O or other oxygen precursors is to employ a metal halide together with a metal alkoxide.[16] The oxygen is derived from the metal alkoxide and alkyl halide elimination produces metal oxide growth. This strategy was originally developed in sol–gel chemistry, which can serve as inspiration for gas phase reactions.[17,18] This chemistry was then applied for gas phase thin film growth using ALD.[19] Waterless processes using this strategy have been developed for the ALD of a variety of oxides including Al$_2$O$_3$,[19,20] Ta$_2$O$_5$,[19,21] hafnium silicate,[22] zirconium silicate,[19,23] and zirconium titanate.[19,24]

Alkyl halide elimination from the reaction of TiCl$_4$ and TTIP has been previously used to deposit TiO$_2$. The sol–gel reaction between TiCl$_4$ and TTIP in anhydrous chloroform has been employed to deposit TiO$_2$ thin films.[25] This

a)Electronic mail: Steven.George@Colorado.Edu

chemistry has been used to modify powdered mesoporous silica materials.[26] There have also been reports of using TiCl$_4$ and TTIP for TiO$_2$ ALD. We discussed the use of TiCl$_4$ and TTIP for TiO$_2$ ALD at the AVS International Symposium in 2010.[27] A recent study has also demonstrated TiO$_2$ ALD using TiCl$_4$ and TTIP.[28]

In this paper, *in situ* transmission Fourier transform infrared (FTIR) spectroscopy was employed to investigate the details of TiO$_2$ ALD using TiCl$_4$ and TTIP. The transmission FTIR experiments were performed on high surface area particle samples that yielded vibrational spectra with high signal-to-noise. The transmission FTIR experiments were able to distinguish the reaction regimes for waterless TiO$_2$ ALD at low and high temperature. In addition, the TiO$_2$ ALD growth rates were determined using quartz crystal microbalance (QCM) measurements and X-ray reflectivity (XRR) studies. The level of chlorine impurities in the TiO$_2$ ALD films was also determined using X-ray photoelectron spectroscopy (XPS) depth-profiling measurements.

II. EXPERIMENTAL METHODS

The TiO$_2$ ALD growth was performed in a viscous flow, warm wall reactor that has been described previously.[29] The reactant precursors were entrained in a flow of nitrogen gas (Airgas UHP grade). Two URS-40 mass flow controllers maintained a N$_2$ flow of 150 sccm. With pumping on the reactor using an Alcatel 2010 C1 mechanical pump, this N$_2$ flow produced a pressure of 1.25 Torr in the reactor. The pressure was measured using a capacitance manometer (MKS).

The *in situ* transmission FTIR experiments were conducted using high surface ZrO$_2$ (Sigma-Aldrich, <50 nm dia.) or SiO$_2$ (Aldrich, ~7 nm dia.) powders samples. These particle samples produced high surface area to increase the signal-to-noise for observing the absorbance of surface species using transmission FTIR experiments. The powders were pressed into a tungsten grid.[30,31] The tungsten grid had 100 lines per inch and a transmission of ~50% for the infrared light. The tungsten grid could be resistively heated to 600 °C using a Love Controls 16 A temperature controller. Resistive heating current was supplied by a programmable Hewlett-Packard 6268B Power supply. A type K thermocouple was used to monitor the temperature.

The FTIR experiments employed a Nicolet model Magna IR 560. The infrared beam was transmitted through CsI windows that were protected from chemical exposure during reactant dosing by gate valves. The infrared detector was a mercury cadmium telluride (MCT-B) detector that was cooled to 77 K with liquid nitrogen. The reactant dosing was controlled using LABVIEW. This electronic control provided consistency in the opening of the pneumatic valves.

The reactants used for the TiO$_2$ deposition were titanium tetrachloride (99.8% TiCl$_4$, Strem Chemicals Inc.) and titanium tetraisopropoxide (TTIP) (99.999% TTIP, Sigma-Aldrich). Both reactants were transferred to their dosing vessels under N$_2$ flow. To ensure adequate vapor pressure, the TTIP source was heated to 50–70 °C during the

experiments. The TiCl$_4$ source was maintained at room temperature.

The *in situ* transmission FTIR studies of TiO$_2$ ALD were performed on ZrO$_2$ powders that were coated with Al$_2$O$_3$ ALD using trimethylaluminum (TMA) (97% pure, Sigma-Aldrich) and H$_2$O (deionized and freeze pump thawed) at 175 °C. The Al$_2$O$_3$ ALD coatings were grown using 10–15 ALD cycles. The Al$_2$O$_3$ ALD coating provided a consistent initial surface for all of the TiO$_2$ ALD experiments in this paper except the FTIR studies of TiO$_2$ ALD films on SiO$_2$ powders. TiO$_2$ ALD coatings could also be deposited directly on the ZrO$_2$ powders.

The SiO$_2$ powders were employed to study the bulk vibrational modes of the TiO$_2$ film because the SiO$_2$ powders have fewer competing bulk vibrational modes. The ZrO$_2$ and SiO$_2$ particles were loaded into the reactor and heated to high temperature to remove surface impurities. The ZrO$_2$ particles were heated to 500 °C, and the SiO$_2$ particles were heated to 350 °C. Water was then used to rehydroxylate the dehydroxylated surfaces prior to the ALD coatings.

A leak valve could be opened to allow some gas to pass into a chamber below the reactor. A quadrupole mass spectrometer system (Stanford Research System Residual Gas Analyzer 200) in this chamber was used for gas analysis. The leak valve was open during the entire quadrupole mass spectrometry (QMS) experiments. A turbomolecular pump (Pfeiffer TPU-062) maintained the lower chamber at pressures below 5×10^{-6} Torr. The turbomolecular pump was backed with a mechanical pump (Alcatel 2005).

QCM experiments were performed in a separate hot wall viscous flow reactor.[32,33] The reactor and samples were all maintained at the reaction temperature with a Eurotherm control. The TiO$_2$ ALD was performed using at pulse sequence of (t$_1$, t$_2$, t$_3$, and t$_4$), where t$_1$ = 5 s TTIP exposure, t$_2$ = 35 s purge, t$_3$ = 1 s TiCl$_4$ exposure, and t$_4$ = 35 s purge. A TM-400 deposition monitor (Inficon/Maxtek, USA) was used to convert the frequency signal (Hz) from the quartz crystal to mass units (ng/cm^2). The TM-400 deposition monitor had a mass resolution of 0.375 ng/cm^2. The gold sputtered, polished, QCM crystals were supplied by Colorado Crystal Corp. (USA).

XRR measurements were performed with a Bede Scientific D1 X-ray diffractometer with a Cu X-ray source. The Cu-Kα beam was monochromated to pass only the Cu-Kα_1 radiation at $\lambda = 1.540$ Å. The filament current was 40 mA, and the electron energy was 40 kV. XPS was performed using a PHI 5600 X-ray photoelectron spectrometer using a monochromatic Al-Kα source. The XPS depth profile measurements were performed using argon ion sputtering.

For the XRR measurements, TiO$_2$ ALD films were deposited on silicon wafers with dimensions of 1 in. × 1 in. Prior to deposition, the silicon substrates were cleaned in a sonicator using acetone and isopropanol. The substrates were allowed to degas in the reactor for at least 30 min prior to deposition. The silicon substrates were then coated with Al$_2$O$_3$ ALD using TMA and H$_2$O prior to the TiO$_2$ ALD with TTIP and TiCl$_4$.

III. RESULTS AND DISCUSSION

A. Surface chemistry during TiCl$_4$ and TTIP reactions

1. In situ *transmission FTIR experiment*

The *in situ* transmission FTIR experiments revealed the surface chemistry during the TiCl$_4$ and TTIP reactions. Figure 1 displays the absolute FTIR spectra for the Al$_2$O$_3$ ALD-coated ZrO$_2$ powders and after the TiCl$_4$ and TTIP exposures for the first two TiO$_2$ ALD cycles on the Al$_2$O$_3$ ALD-coated ZrO$_2$ particles at 150 °C. The FTIR spectrum for the Al$_2$O$_3$ ALD-coated ZrO$_2$ powders was referenced to the clean and hydroxylated ZrO$_2$ powders. The FTIR spectra after the TiCl$_4$ and TTIP exposures were referenced to the starting Al$_2$O$_3$ ALD surface.

Figure 1(a) exhibits the hydroxyl terminated surface after 15 Al$_2$O$_3$ ALD cycles. There are two types of hydroxyl stretches: the isolated AlO-H stretches at ~3750 cm^{-1} and the hydrogen-bonded AlO-H stretches between 2600 and 3700 cm^{-1}. Figure 1(b) shows the loss of hydroxyl species at ~3750 cm^{-1} after the 1st TiCl$_4$ exposure. This loss is consistent with the reaction of TiCl$_4$ with the isolated Al-OH species on the initial Al$_2$O$_3$ ALD surface. These Al-OH species at ~3750 cm^{-1} are the free hydroxyl groups that are not hydrogen-bonded to each other. Similar results were observed in a previous FTIR study of TiO$_2$ ALD on ZrO$_2$ particles using TiCl$_4$ and H$_2$O.[34]

Figure 1(b) also shows that the hydrogen-bonded Al-OH species are not lost between ~2600 and 3700 cm^{-1} during TiCl$_4$ exposures. The lack of a negative absorbance after referencing to the initial Al$_2$O$_3$ ALD surface indicates that these hydrogen-bonded hydroxyl groups do not react readily

with TiCl$_4$. The growth of Ti-Cl vibrational features is not observed in Fig. 1(b) because the frequency of the Ti-Cl vibrational modes is below the cutoff frequency of the detector. The Ti-Cl stretching vibrational frequency is between 400 and 450 cm^{-1} in various titanium chloride complexes.[35] The Ti-Cl stretching vibrational frequency is ~500 cm^{-1} in TiCl$_4$.[36]

The FTIR spectrum after the first TTIP exposure is shown in Fig. 1(c). This spectrum is also referenced to the initial Al$_2$O$_3$ ALD surface. Consequently, the loss of Al-OH species at ~3750 cm^{-1} remains in the FTIR spectrum. In addition, prominent new absorbance features appear at 2850–3000 cm^{-1} that are assigned to C-H stretches. Additional absorbance features also are present at 1300–1480 cm^{-1} that are assigned to CH$_x$ bends. Strong absorbance features at 1020 and 1130 cm^{-1} are also assigned to CO symmetric and antisymmetric stretching modes. These peak identifications are based on earlier assignments in the literature.[5,37] These absorbance features are consistent with isopropoxide groups on the surface.

The FTIR spectra after the second TiCl$_4$ and TTIP exposures are shown in Figs. 1(d) and 1(e). These spectra are very similar to the spectra in Figs. 1(b) and 1(c). These similar spectra indicate that the TiO$_2$ ALD reactions occurring during the sequential TiCl$_4$ and TTIP exposures are very consistent. This consistency suggests that the nucleation of the TiO$_2$ ALD on the Al$_2$O$_3$ ALD surface occurs without difficulty.

The FTIR spectra in Figs. 2(a) and 2(b) show the TiCl$_4$-TTIP and TTIP-TiCl$_4$ difference spectra corresponding to the second cycle during TiO$_2$ ALD. The spectrum after the TiCl$_4$ exposure in Fig. 2(a) is referenced to the spectrum after
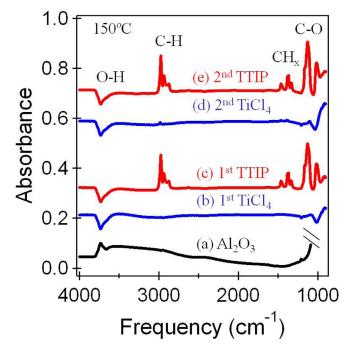

FIG. 1. (Color online) FTIR spectra before and after the first two TiO$_2$ ALD cycles on Al$_2$O$_3$ ALD-coated ZrO$_2$ particles at 150 °C. The Al$_2$O$_3$ spectrum is referenced to the hydroxylated ZrO$_2$ particles. The spectra during TiO$_2$ ALD are referenced to the spectrum of initial Al$_2$O$_3$ ALD-coated ZrO$_2$ particles.
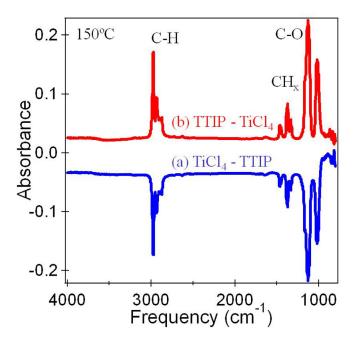
FIG. 2. (Color online) Difference FTIR spectra during the second cycle of TiO$_2$ ALD on Al$_2$O$_3$ ALD-coated ZrO$_2$ particles at 150 °C. (a) FTIR spectrum after the TiCl$_4$ exposure referenced to the FTIR spectrum after the previous TTIP exposure. (b) FTIR spectrum after the TTIP exposure referenced to the FTIR spectrum after the previous TiCl$_4$ exposure.

the TTIP exposure. The spectrum after the TTIP exposure in Fig. 2(b) is referenced to the spectrum after the TiCl₄ exposure. These difference spectra emphasize the vibrational features that are lost or gained with the TiCl₄ and TTIP exposures. The C-H stretching and bending vibrations and C-O stretching vibrations that are associated with the isopropoxide surface species are lost after the TiCl₄ exposure. These features are then added back after the TTIP exposure.

The spectra in Figs. 2(a) and 2(b) are near mirror images of each other. This symmetry reflects the consistent, self-limiting chemistry during these TiO₂ ALD reactions. There is also no indication of any hydroxyl species being produced or lost during the reactions at 150 °C. The lack of hydroxyl species is consistent with the stability of an isopropoxide species that does not undergo any β-hydride elimination at 150 °C. The spectra in Figs. 1 and 2 are consistent with a reaction mechanism at low temperature that is illustrated in Figs. 3 and 4. Figure 3 shows the reaction mechanism during the TTIP reaction. Figure 4 shows the reaction mechanism during the TiCl₄ reaction.

The reaction mechanisms shown in Figs. 3 and 4 occur without the production of a surface hydroxyl species. The reaction of TTIP with the =TiCl₂ surface species can be viewed as resulting from the nucleophilic attack by an oxygen in TTIP on the electropositive Ti in the =TiCl₂ surface species. Chlorine transfer to the isopropyl group to form 2-chloropropane is concurrent with the formation of a Ti-O bond. During the TiCl₄ reaction, the oxygen of the isopropyl group on the surface again undergoes nucleophilic attack on
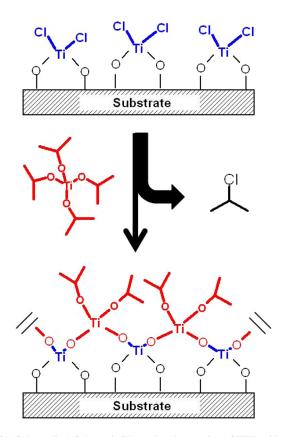

FIG. 4. (Color online) Schematic illustrating the reaction of TiCl₄ with isopropoxide surface species to yield TiCl₂ surface species and 2-chloropropane.

the electropositive Ti in the TiCl₄ reactant. Chlorine transfer to the isopropyl group to form 2-chloropropane is again concurrent with the formation of a Ti-O bond.

Figure 5 displays the FTIR spectra after the TiCl₄ and TTIP exposures for the first two TiO₂ ALD cycles on the Al₂O₃ ALD-coated ZrO₂ particles at 275 °C. Each FTIR

FIG. 3. (Color online) Schematic illustrating the reaction of TTIP with TiCl₂ surface species to yield isopropoxide surface species and 2-chloropropane.
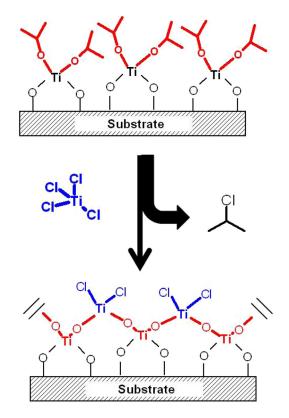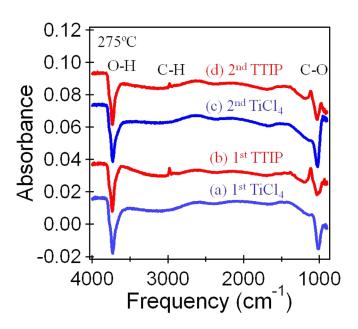

FIG. 5. (Color online) FTIR spectra after the first two TiO₂ ALD cycles on Al₂O₃ ALD-coated ZrO₂ particles at 275 °C. The FTIR spectra are all referenced to the spectrum of the initial Al₂O₃ ALD-coated ZrO₂ particles.

spectrum was referenced to the starting Al$_2$O$_3$ ALD surface. Figure 5(a) was recorded after the first TiCl$_4$ exposure and shows the loss of hydroxyl species at ~3750 cm^{-1}. This loss is similar to the loss observed in Fig. 1(a) and is consistent with the reaction of TiCl$_4$ with free hydroxyl groups that are not hydrogen-bonded to each other. Figure 5(a) also shows that some of the hydrogen-bonded Al-OH species are lost between ~3400 and 3700 cm^{-1}. The hydrogen-bonded Al-OH species are more likely to react with TiCl$_4$ at the higher temperature of 275 °C.

The FTIR spectrum after the first TTIP exposure is shown in Fig. 5(b). This spectrum is also referenced to the initial Al$_2$O$_3$ ALD surface, and the loss of Al-OH species at ~3750 cm^{-1} remains in the FTIR spectrum. Figure 5(b) does not observe significant absorbance for C-H stretching and bending vibrational modes that would be associated with isopropoxide species. The comparison between the FTIR spectra in Figs. 1(b) and 5(b) is dramatic. The absence of the C-H stretching and bending vibrational modes in Fig. 5(b) indicates that the isopropoxide species are not stable at 275 °C.

The hydroxyl region appears to be relatively unchanging in the FTIR spectra in Fig. 5. This region of the spectrum is dominated by the loss of the Al-OH species from the Al$_2$O$_3$ ALD surface. However, changes in the hydroxyl region are much more apparent in the FTIR spectra shown in Fig. 6. The FTIR spectra in Figs. 6(a) and 6(b) show the TiCl$_4$-TTIP and TTIP-TiCl$_4$ difference spectra corresponding to the second cycle during TiO$_2$ ALD. The spectrum after the TiCl$_4$ exposure in Fig. 6(a) is referenced to the spectrum after the TTIP exposure. The spectrum after the TTIP exposure in Fig. 6(b) is referenced to the spectrum after the TiCl$_4$ exposure.
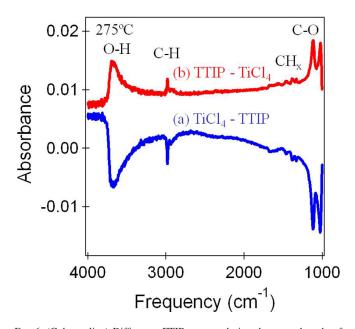
Figure 6(a) shows that the TiCl$_4$ exposure at 275 °C removes hydroxyl groups from surfaces previously exposed to TTIP. Figure 6(b) shows that the TTIP exposure at 275 °C adds hydroxyl groups to the surface produced by the TiCl$_4$ exposure. The addition of hydroxyl groups in Fig. 6(b) following the TTIP exposure is consistent with the isopropoxide species undergoing β-hydride elimination to yield propene and surface hydroxyl groups at 275 °C. Figure 7 presents an illustration of β-hydride elimination of the isopropoxide surface species and the production of hydroxyl groups. TiCl$_4$ then reacts with the hydroxyl groups and forms $=$TiCl$_2$ groups on the surface. The recent study of TiO$_2$ ALD using TiCl$_4$ and TTIP also obtained evidence for a β-hydride elimination reaction.[28] However, this recent study did not observe any hydroxyl groups.[28]

The complete reaction mechanism for TiO$_2$ ALD at 275 °C includes the reaction of TTIP with TiCl$_2$ surface species as shown in Fig. 3. The isopropoxide species then undergo β-hydride elimination to produce surface hydroxyl groups as shown in Fig. 7. These hydroxyl groups can then easily react with TiCl$_4$ to re-form the $=$TiCl$_2$ surface species and HCl as the gaseous reaction product.

FIG. 6. (Color online) Difference FTIR spectra during the second cycle of TiO$_2$ ALD on Al$_2$O$_3$ ALD-coated ZrO$_2$ particles at 275 °C. (a) FTIR spectrum after the TiCl$_4$ exposure referenced to the FTIR spectrum after the previous TTIP exposure. (b) FTIR spectrum after the TTIP exposure referenced to the FTIR spectrum after the previous TiCl$_4$ exposure.
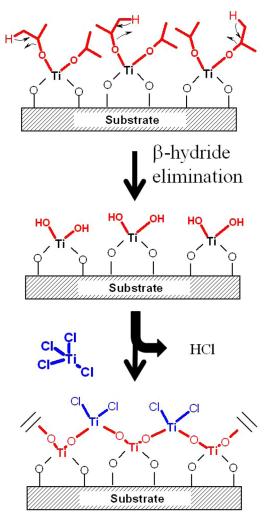

FIG. 7. (Color online) Schematic illustrating β-hydride elimination of the isopropoxide surface species to yield hydroxyl surface species. The hydroxyl surface species then react with TiCl$_4$ to yield TiCl$_2$ surface species and HCl.
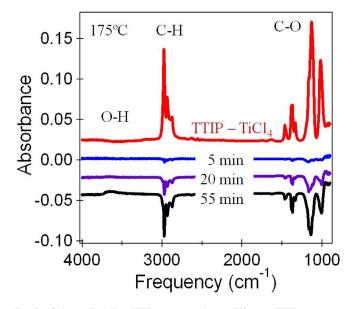
FIG. 8. (Color online) Top FTIR spectrum shows difference FTIR spectrum after TTIP exposure at 175 °C on the surface previous exposed to TiCl$_4$. The descending FTIR spectra show difference FTIR spectra vs time at 175 °C referenced to the top FTIR spectrum.

FTIR spectra recorded at different times followed the loss of the isopropoxide features at various temperatures. Figure 8 shows the FTIR spectrum after a TTIP exposure at 175 °C. This FTIR spectrum was referenced to the FTIR spectrum after the previous TiCl$_4$ exposure. This spectrum is very similar to the spectrum in Fig. 2(b). The FTIR spectra were then recorded versus time and referenced to the initial TTIP-TiCl$_4$ FTIR spectrum to monitor the stability of the isopropoxide species.

The loss of the isopropoxide species resulting from β-hydride elimination leads to the loss of C-H stretching and bending features and C-O vibrational features. The difference FTIR spectra after 5, 20, and 55 min are shown in Fig. 8. In addition to the loss of the isopropoxide species, Fig. 8 also reveals the growth of a small hydroxyl peak at ~3500–3750 cm^{-1} after 55 min. The appearance of this hydroxyl peak is consistent with a β-hydride elimination reaction that produces hydroxyl species and propene. This hydroxyl feature could be caused by H$_2$O adsorption onto the growing TiO$_2$ surface. To rule out this possibility, the FTIR spectrum was monitored for two hours after a TiCl$_4$ reaction at 150 °C. No hydroxyl features grew in the hydroxyl region at 3500–3750 cm^{-1}. The absence of hydroxyl groups in this experiment argues that the hydroxyl groups in Fig. 8 result from a β-hydride elimination reaction.

To monitor the time-dependence of the isopropoxide features at various temperatures, Fig. 9 shows the integrated absorbance of the C-H stretching vibrational modes at ~2975 cm^{-1} after various times. The collection of the integrated absorbance began after the sample reached the experimental temperature. The initial integrated absorbances are smaller at higher temperatures because more integrated absorbance was lost at higher temperatures before the FTIR scans could quantify the integrated absorbance. A simple analysis of the initial slopes of the integrated absorbance
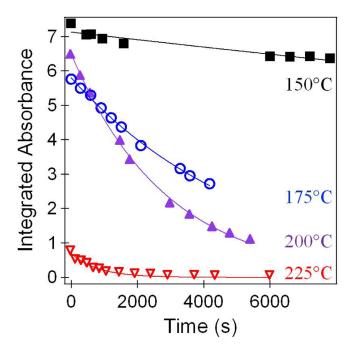

FIG. 9. (Color online) Integrated absorbance of the C-H stretching vibrational modes of the isopropoxide surface species at ~2975 cm^{-1} vs time at 150, 175, 200, and 225 °C. The time t = 0 is defined when the sample reaches the temperature.

versus time yielded relative loss rates. An Arrhenius plot of these loss rates yielded an estimated activation barrier of 15 ± 2 kcal/mole for the β-hydride elimination reaction.

B. Quadrupole mass spectrometry experiment

To confirm the β-hydride elimination mechanism, quadrupole mass spectrometry was utilized to monitor the gas phase species during and after the TTIP reaction. Propene is the expected gas phase reaction product during β-hydride elimination reaction. The most intense mass cracking fragment for propene is at m/z = 41. This mass fragment was used to monitor propene. However, the mass cracking pattern of TTIP, isopropanol, and 2-chloropropane all produce signals at m/z = 41. Because of this overlap, various mass fragments from the possible gas molecules were examined before, during, and after the TTIP reaction to confirm the presence of propene.

The gas molecules that were examined were propene, isopropanol, 2-chloropropane, TiCl$_4$, and TTIP. The mass cracking patterns of these gases were examined and compared with the expected mass cracking patterns in the database of the National Institute of Standards and Technology (NIST). All of the gases produced mass cracking patterns similar to the NIST database. TTIP has its most intense mass cracking peak at m/z = 45. Therefore, if the m/z = 41 and m/z = 45 signals are monitored and the m/z = 41 signal increased but not m/z = 45 signal, the gas phase species is not TTIP. 2-chloropropane has its most intense mass cracking peak at m/z = 43.

After characterizing the mass cracking patterns of the reactants and the most likely products of the surface reactions or the β-hydride elimination reaction, the mass signals

were monitored during and after the TTIP and TiCl₄ reactions at 225 °C. The reactants and products were clearly observed using static dosing of the reactants. Small amounts of the reactants were introduced into the reactor with the valve closed to the mechanical pump. Gases were transmitted through the leak valve to the chamber containing the mass spectrometer. After each reactant exposure and time after the reactant exposure, the mechanical pump evacuated the reactor chamber prior to the next reactant exposure.

TiCl₄ exposures on surfaces at 225 °C previously exposed to TTIP yielded a strong signal at m/z = 36 and 38. These mass fragments are the expected mass signals for HCl, and they appeared with relative intensities as expected from their chlorine isotopic abundance. The HCl species indicates that hydroxyl groups are present because HCl is the reaction product of TiO₂ ALD using TiCl₄ and H₂O. TTIP exposures on surfaces previously exposed to TiCl₄ produced signals at m/z = 41 and 43. There was no signal at m/z = 45, indicating that all the parent was reacted to produce reaction products. Subsequently, the signal at m/z = 41 continued to rise while the signal at m/z = 43 was constant. These results are consistent with the production of 2-chloropropane reaction product at m/z = 43. The initial signal at m/z = 41 results from the production of 2-chloropropane and possibly some propene. The signal at m/z = 41 continues to grow because of the production of propene by the β-hydride elimination reaction. The signal at m/z = 41 persisted even after the evacuation of the reactor.

Further TTIP dosing will eventually lead to the saturation of the TTIP reaction. At the point of saturation, TTIP should be observed in the mass spectrum. Figure 10 shows the results for m/z = 41 and m/z = 45 for sequential TTIP exposures at 225 °C. The signals for m/z = 45 have been offset slightly to avoid overlap with the signals at m/z = 41. The

first TTIP produces mostly mass signal at m/z = 41 that corresponds to 2-chloropropane and possibly some propene. The negligible signal at m/z = 45 indicates that all of the TTIP is consumed to produce reaction products.

The results are very similar for the second sequential TTIP exposure. These results are expected if the TTIP reaction has not reached saturation. The signal at m/z = 41 again corresponds to 2-chloropropane and possibly some propene. The third TTIP leads to the appearance of mass signal at m/z = 45. This signal results from TTIP and indicates that the TTIP reaction has reached completion. Additional TTIP exposures now all produce signal at m/z = 45 because the reaction is self-limiting and TTIP can reach the mass spectrometer.

1. Growth of the TiO₂ ALD Film

QCM analysis was performed to measure the growth of the TiO₂ ALD films. Results for QCM experiments at 150 °C and 250 °C under the same reaction conditions are shown in Fig. 11. The mass gain is linear versus time indicating a consistent mass deposition with each TiO₂ ALD cycle that occurs every 76 s. The growth rate is only 3 ng/cm² at 150 °C. The growth rate increases to 15 ng/cm² at 250 °C. This large difference in growth rate at 150 °C and 250 °C is attributed to the difference in reaction mechanism.

At 150 °C, the isopropoxide species does not undergo β-hydride elimination. The TiCl₄ is forced to react with the isopropoxide species on the surface. At 250 °C, the isopropoxide species can undergo β-hydride elimination and produce hydroxyl surface species. The larger growth rate at 250 °C suggests that the TiCl₄ can react more easily with these hydroxyl species. The QCM mass gain at 250 °C shows changes during the individual reactant exposures that are attributed to transient temperature effects.[38] Temperature transients can cause false mass change transients without influencing the overall mass gain.[38]
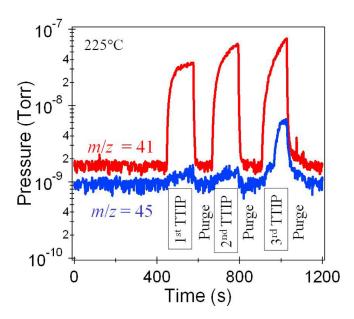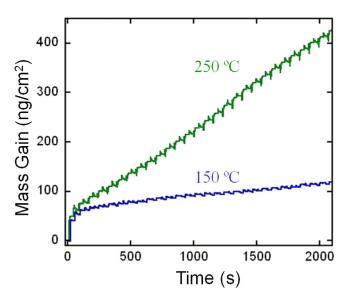

FIG. 10. (Color online) Quadrupole mass spectrometry results showing the mass signals at m/z = 41 and m/z = 45 vs time during three sequential TTIP exposure and purge sequences at 225 °C. The mass signal at m/z = 41 is attributed primarily to 2-chloropropane. The mass signal at m/z = 45 is attributed primarily to TTIP.

FIG. 11. (Color online) Quartz crystal microbalance results during TiO₂ ALD showing mass gain vs time at 150 and 250 °C.
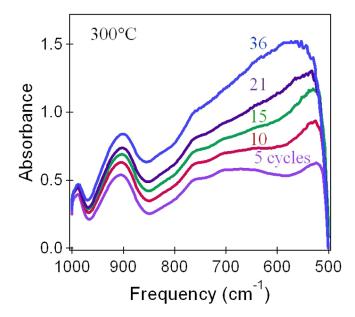
FIG. 12. (Color online) FTIR spectra in the low frequency region from 500 to 1000 cm^{-1} showing the bulk vibrational modes of TiO$_2$ vs number of TiO$_2$ ALD cycles on SiO$_2$ particles at 300 °C.
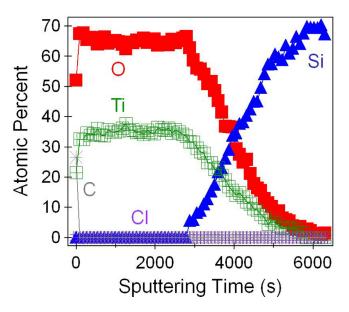

FIG. 13. (Color online) X-ray photoelectron spectra during depth-profiling of a TiO$_2$ ALD film grown on a silicon wafer using 100 TiO$_2$ ALD cycles at 250 °C. The TiO$_2$ ALD film had an initial thickness of ∼55 Å.

XRR analysis was also employed to quantify the growth of the TiO$_2$ ALD films. For TiO$_2$ ALD films grown on Al$_2$O$_3$ ALD-coated silicon wafers, the growth rate was 0.55 ± 0.05 Å/cycle at 250 °C. In comparison, using the density of 3.3 g/cm^3 for the TiO$_2$ ALD film determined by XRR, the mass gain of 15 ng/cm^2 at 250 °C was consistent with a growth rate of 0.5 Å/cycle. These XRR and QCM results are in excellent agreement. This growth rate is also somewhat lower than the growth rate of 0.7 Å/cycle measured by recent ellipsometry studies.[28]

TiO$_2$ ALD growth can also be observed in the FTIR spectra. For these experiments, TiO$_2$ ALD was performed on SiO$_2$ particles. The SiO$_2$ particles have a favorable bulk vibrational absorbance that provides a window to observe the TiO$_2$ ALD film growth. Figure 12 shows the FTIR spectra in the frequency region between 500 and 1000 cm^{-1}. One absorbance peak is observed between 850 and 950 cm^{-1}. Another broad absorbance peak is observed at ∼500–750 cm^{-1}. This peak may be a shoulder of an absorbance peak with its maximum absorbance at <500 cm^{-1} because the infrared detector employed in these experiments does not respond below 500 cm^{-1}. The breadth of these peaks suggests the partial amorphous nature of the TiO$_2$ film.[39]

The absorbance spectra in Fig. 12 is similar to the absorbance of TiO$_2$ films deposited using plasma-enhanced chemical vapor deposition (PE-CVD) with TiCl$_4$ and O$_2$.[39] These PECVD TiO$_2$ films were amorphous and displayed no XRD peaks after deposition at <65 °C. The PECVD TiO$_2$ films began to display crystallinity consistent with anatase TiO$_2$ after annealing at 600 °C. The absorbance in the region of 700–950 cm^{-1} has been assigned to longitudinal optical (LO) vibration of the Ti-O bonds in the TiO$_2$ film.[39] The absorbance in the region of 400–600 cm^{-1} has been assigned to transverse optical (TO) vibration of the Ti-O bonds.[39]

Figure 12 shows that the two absorbance features grow progressively with number of TiO$_2$ ALD cycles. This behavior argues that these peaks are associated with the TiO$_2$ ALD film. In addition, the absorption peak between 850 and 950 cm^{-1} may be influenced by the formation of an aluminum titanate. A previous infrared study of TiO$_2$/SiO$_2$ multilayers observed a peak at 930 cm^{-1} that was assigned to Si-OTi species.[40] This absorbance peak was observed only in the composite TiO$_2$/SiO$_2$ films.[40]

Ex situ XPS analysis was also employed to determine the elemental composition of the TiO$_2$ ALD films. Figure 13 shows the depth profile results for TiO$_2$ ALD films with a thickness of ∼55 Å that was grown using 100 TiO$_2$ ALD cycles at 250 °C. Titanium and oxygen are in their expected ratio of ∼1:2. At longer sputtering times, the XPS signal for the underlying silicon wafer begins to appear and then dominates the XPS signals. There is adventitious carbon on the surface. However, the carbon XPS signal quickly is reduced to below the detection limit of 1 at. % versus sputtering time. In addition, there is no detectable chlorine in the TiO$_2$ ALD films. Therefore, any residual chlorine in the TiO$_2$ ALD films is below the detection limit of 1 at. %.

The XRR analysis of TiO$_2$ ALD films grown at 250 °C with thicknesses <70 Å were very smooth with an RMS roughness of ∼5 Å or less. The roughness determined by XRR analysis increased for film thicknesses >100 Å. The RMS roughness was ∼30 Å for TiO$_2$ ALD films grown at 250 °C with a thickness of 110 Å. An X-ray diffraction (XRD) analysis also showed that the thicker TiO$_2$ ALD films grown at 250 °C displayed diffraction peaks consistent with at least a partial anatase TiO$_2$ crystal structure.

IV. CONCLUSIONS

Waterless TiO$_2$ ALD was achieved using TiCl$_4$ and TTIP as the reactants. The surface species and the reactions during

waterless TiO$_2$ ALD were examined using *in situ* transmission FTIR studies. The FTIR absorbance spectra showed that the isopropoxide species remained on the surface after TTIP exposures at low temperatures between 125 and 225 °C. The TiCl$_4$ exposures then removed the isopropoxide species and deposited titanium species. The isopropoxide species were converted to hydroxyl species by β-hydride elimination at high temperatures between 250 and 300 °C. The β-hydride elimination reaction pathway was confirmed by the observation of propene by QMS. The TiCl$_4$ exposures then reacted with the hydroxyl species. QMS measurements also detected the 2-chloropropane and HCl gaseous reaction products and observed the self-limiting nature of the TTIP reaction.

The waterless TiO$_2$ ALD growth at low and high temperature was also examined by additional studies. At a low temperature of 150 °C, QCM measurements observed growth rates of $\sim$3 ng/cm^2. Much higher growth rates of $\sim$15 ng/cm^2 were measured at a higher temperature of 250 °C. XRR analysis obtained a growth rate of 0.55 ± 0.05 Å/cycle at 250 °C. XPS depth-profile studies revealed that the TiO$_2$ films contained low Cl concentrations <1 at. %. The waterless TiO$_2$ ALD surface chemistry using TiCl$_4$ and TTIP may restrict surface oxidation during TiO$_2$ ALD on oxygen-sensitive substrates.

ACKNOWLEDGMENTS

[1]M. Ritala, M. Leskela, E. Nykanen, P. Soininen, and L. Niinisto, Thin Solid Films **225**, 288 (1993).
[2]M. Ritala, M. Leskela, L. Niinisto, and P. Haussalo, Chem. Mater. **5**, 1174 (1993).
[3]Q. Xie, Y. L. Jiang, C. Detavernier, D. Deduytsche, R. L. Van Meirhaeghe, G. P. Ru, B. Z. Li, and X. P. Qu, J. Appl. Phys. **102**, 083521 (2007).
[4]J. Aarik, A. Aidla, T. Uustare, M. Ritala, and M. Leskela, Appl. Surf. Sci. **161**, 385 (2000).
[5]V. R. Rai and S. Agarwal, J. Phys. Chem. C **112**, 9552 (2008).
[6]K. B. Ramos, G. Clavel, C. Marichy, W. Cabrera, N. Pinna, and Y. J. Chabal, Chem. Mater. **25**, 1706 (2013).
[7]Y. W. Kim and D. H. Kim, Korean J. Chem. Eng. **29**, 969 (2012).
[8]M. Rose, J. Niinisto, P. Michalowski, L. Gerlich, L. Wilde, I. Endler, and J. W. Bartha, J. Phys. Chem. C **113**, 21825 (2009).
[9]S. E. Potts, W. Keuning, E. Langereis, G. Dingemans, M. C. M. van de Sanden, and W. M. M. Kessels, J. Electrochem. Soc. **157**, P66 (2010).
[10]M. Schuisky, K. Kukli, J. Aarik, J. Lu, and A. Harsta, J. Cryst. Growth **235**, 293 (2002).
[11]P. Bernhard, C. Ziethen, R. Ohr, H. Hilgers, and G. Schonhense, Surf. Coat. Technol. **180**, 621 (2004).
[12]V. Novotny, G. Itnyre, A. Homola, and L. Franco, IEEE Trans. Magn. **23**, 3645 (1987).
[13]P. Gupta, A. C. Dillon, A. S. Bracker, and S. M. George, Surf. Sci. **245**, 360 (1991).
[14]M. K. Weldon, B. B. Stefanov, K. Raghavachari, and Y. J. Chabal, Phys. Rev. Lett. **79**, 2851 (1997).
[15]J. Robertson, Rep. Prog. Phys. **69**, 327 (2006).
[16]P. H. Mutin and A. Vioux, Chem. Mater. **21**, 582 (2009).
[17]R. J. P. Corriu, D. Leclercq, P. Lefevre, P. H. Mutin, and A. Vioux, J. Mater. Chem. **2**, 673 (1992).
[18]G. Clavel, E. Rauwel, M.-G. Willinger, and N. Pinna, J. Mater. Chem. **19**, 454 (2009).
[19]M. Ritala, K. Kukli, A. Rahtu, P. I. Raisanen, M. Leskela, T. Sajavaara, and J. Keinonen, Science **288**, 319 (2000).
[20]P. I. Raisanen, M. Ritala, and M. Leskela, J. Mater. Chem. **12**, 1415 (2002).
[21]K. Kukli, M. Ritala, and M. Leskela, Chem. Mater. **12**, 1914 (2000).
[22]W. K. Kim, S. W. Rhee, N. I. Lee, J. H. Lee, and H. K. Kang, J. Vac. Sci. Technol. A **22**, 1285 (2004).
[23]W. K. Kim, S. W. Kang, S. W. Rhee, N. I. Lee, J. H. Lee, and H. K. Kang, J. Vac. Sci. Technol. A **20**, 2096 (2002).
[24]A. Rahtu, M. Ritala, and M. Leskela, Chem. Mater. **13**, 1528 (2001).
[25]P. Arnal, R. J. P. Corriu, D. Leclercq, P. H. Mutin, and A. Vioux, Chem. Mater. **9**, 694 (1997).
[26]W. F. Yan, S. M. Mahurin, S. H. Overbury, and S. Dai, Chem. Mater. **17**, 1923 (2005).
[27]V. R. Anderson, A. S. Cavanagh, A. I. Abdulagatov, Z. M. Gibbs, and S. M. George, "Waterless TiO₂ atomic layer deposition using titanium tetrachloride and titanium tetraisopropoxide," *Presented at AVS 57th International Symposium & Exhibition*, Albuquerque Convention Center, Albuquerque, NM, 19 October 2010.
[28]R. P. Chaukulkar and S. Agarwal, J. Vac. Sci. Technol. A **31**, 031509 (2013).
[29]D. N. Goldstein, J. A. McCormick, and S. M. George, J. Phys. Chem. C **112**, 19530 (2008).
[30]T. H. Ballinger, J. C. S. Wong, and J. T. Yates, Langmuir **8**, 1676 (1992).
[31]J. D. Ferguson, A. W. Weimer, and S. M. George, Thin Solid Films **371**, 95 (2000).
[32]A. I. Abdulagatov, R. A. Hall, J. L. Sutherland, B. H. Lee, A. S. Cavanagh, and S. M. George, Chem. Mater. **24**, 2854 (2012).
[33]J. W. Elam, M. D. Groner, and S. M. George, Rev. Sci. Instrum. **73**, 2981 (2002).
[34]J. D. Ferguson, A. R. Yoder, A. W. Weimer, and S. M. George, Appl. Surf. Sci. **226**, 393 (2004).
[35]A. Gomezcarrera, M. Mena, P. Royo, and R. Serrano, J. Organomet. Chem. **315**, 329 (1986).
[36]W. B. Person and W. B. Maier, J. Chem. Phys. **69**, 297 (1978).
[37]P. D. Moran, G. A. Bowmaker, R. P. Cooney, K. S. Finnie, J. R. Bartlett, and J. L. Woolfrey, Inorg. Chem. **37**, 2741 (1998).
[38]M. N. Rocklein and S. M. George, Anal. Chem. **75**, 4975 (2003).
[39]T. Busani and R. A. B. Devine, Semicond. Sci. Technol. **20**, 870 (2005).
[40]T. Nakayama, J. Electrochem. Soc. **141**, 237 (1994).